Metallography, Microstructure, and Analysis (2022) 11:327–340
https://doi.org/10.1007/s13632-022-00848-9

PEER REVIEWED

Corrosion Behavior of the 6061 Al–Mg–Si Alloy in Different Soils Extracts

Mariana Xavier Milagre[1] · João Victor de Sousa Araujo[1] · Caruline de Souza Carvalho Machado[2] · Marco Stanojev Pereira[1] · Renato Altobelli Antunes[3] · Frederico Genezini[1] · Isolda Costa[1]

Received: 6 January 2022 / Revised: 19 April 2022 / Accepted: 25 April 2022 / Published online: 11 May 2022

Abstract
In this work, the corrosion behavior of the 6061 Al-alloy in different temper conditions was studied in different soil extracts using electrochemical and surface monitoring techniques. The results showed that the corrosion behavior of the 6061 alloy depends on the soil extract composition, with the highest electrochemical activities related to the soil extracts with the lowest nitrate and sulfate concentrations. The 6061-T6 condition was more susceptible to corrosion than the 6061-HCR one. The results were related to the higher amounts of MgSi particles in the 6061-T6 alloy compared to the 6061-HCR. Sulfate and nitrate ions acted as corrosion inhibitor reducing the corrosion kinetics of the 6061 alloy in solutions with high concentration of chloride ions.

Keywords Aluminum alloys · Localized corrosion · Characterization · Soil extract corrosion

Introduction

The 6061 Al–Mg–S Al-alloy i is a versatile alloy which can be applied in trucks, towers, canoes, railroads cars, furniture, pipelines, nuclear reactor structures, and other applications where strength, weldability, and corrosion resistance are essential properties [1]. This alloy is applied as buried structural components and cladding due to its corrosion resistance compared with alloys from the other Al series. For structural applications, the 6061 is generally used in the T6 temper condition. This is the peak age condition in which the alloy presents improved mechanical properties due to precipitation of the β″ phase [2–4]. On the other hand, the cladding produced by a sequence of heating, hot and cold rolling (HCR) steps [5, 6] and this process has been reported to change the microstructural feature and corrosion behavior of the 6061 alloy [7, 8].

Since the buried 6061 alloy can be exposed to different environments depending on its application, it is important to understand the impact of the environment on the corrosion of the 6061 alloy, for instance, the corrosiveness of the soil nature. The soil composition is highly complex, and therefore the causes of its corrosiveness are difficult to be established. In general, the soil properties which affect the corrosion resistance of buried structures are its redox potential, pH, chemical composition, sulfate and chloride contents, presence of sulfide reducing bacteria, and resistivity. Soil resistivity, for instance, regulates the electric current between anodic and cathodic sites that promote corrosion. For Al-alloys, a soil resistivity of 1500 Ω cm has been suggested as the value below which the alloys are susceptible to corrosion. Similarly, according to the soil pH, the buried structure can be immune to corrosion. According to the literature [9, 10], Al alloys are passive in pH range of 4–9.

The corrosion behavior of buried Al alloys is also determined by the soil texture [11]. Severe corrosion has been associated with heterogeneous soil, either alkaline or acid, whereas slight corrosion is reported in neutral or acid clay homogeneous soil [11]. Yan et al. [12] studied the corrosion behavior of an Al alloy immersed in alkaline soil extracts. According to the authors, the alloy was susceptible to pitting

✉ Mariana Xavier Milagre
marianamilagre@yahoo.com.br

1 Instituto de Pesquisas Energéticas e Nucleares – IPEN/CNEN, Av. Prof. Lineu Prestes, São Paulo 2242, Brazil

2 Departamento. de Engenharia Metalúrgica e de Materiais, Universidade de São Paulo, São Paulo 05508-030, Brazil

3 Centro de Engenharia, Modelagem e Ciências Sociais Aplicadas, Universidade Federal do ABC, Av. dos Estados, Santo André 5001, Brazil

and exfoliation corrosion, as well as the corrosion products, were mainly aluminum oxides and sulfides. In another work, the authors reported that Al alloys for use as grounding material, when in contact with alkaline soil of high chloride content, are susceptible to pitting and intergranular corrosion due to the aggressiveness of chloride ions [13].

In this work, the corrosion behavior of the 6061 alloy in two temper conditions, T6 and HCR, was studied in different soil extracts. The corrosion behavior was monitored by optical and scanning electron microscopy and the corrosion resistance was evaluated by electrochemical techniques. Different behaviors were observed for both alloys depending on the soil extract characteristics.

Experimental

Material

The material used in this study was the 6061 alloy (Al 89.9 wt.%, Cr 0.10 wt.%, Cu 0.22%, Fe 0.20 wt.%, Mg 0.90 wt.%, Mn 0.05 wt.%, Si 0.13 wt.%, and Zn 0.02 wt.%) in two thermomechanical conditions. The first was the T6 one which comprises stages of solution heat treatment and artificial aging. The second condition was named HCR. The HCR condition corresponds to a sequence of heating at 440 °C for 15 min, 2–3 hot passes of rolling, heating at 440 °C for 15 min, 7–9 passes of hot rolling, heating at 440 °C for 60 min and, finally, 1–2 passes of cold rolling.

Soil Extracts

Three different soil samples collected from different regions were used in this study. They were dried at 100 °C, in an oven, for 2 days. Subsequently, the samples were sieved through a 70 mesh sieve. The soils extract solutions were made using 200 g of the fine portion of the soil and then adding water until a volume of 1 L. The solutions were left in agitation for 1 day and, then, filtered. The composition of the soil extracts was analyzed by ICP-OES, Table 1.

Samples Preparation and Characterization

The surface of the samples for exposure to the test solution was prepared by sequentially grinding with SiC emery papers (#500, #800, #1200, #2500, #4000). Subsequently, the samples were immersed in 10 wt.% NaOH at 60 °C for 1 min, and then, exposed to 30 vol.% HNO_3 solution for 1 min. Finally, the surface-treated samples were rinsed in deionized water and dried. The surface for exposure to corrosion tests was examined, before and after tests, by optical microscopy and analyzed by scanning electron microscopy using a Hitachi TM 3000 with an incident beam of 15 keV coupled with Energy Dispersive X-ray Spectroscopy (EDX). The corroded surface was characterized using an ZYGO's ZeGage™ 3D optical profilometry and also Neutron Tomography facility installed at IEA—R1 Nuclear Research Reactor, located at the Instituto de Pesquisas Energéticas e Nucleares (IPEN), in the city of São Paulo. References [14–16] describe in detail, the equipment, and the procedures used for tomography.

Table 1 Properties of the soil extracts used in this study (chemical composition, conductivity and pH)

Íon, mg L^{-1}	Soil 1	Soil 2	Soil 3
F^-	0.11 ± 0.001	< 0.10	0.343 ± 0.003
Br^-	< 0.5	< 0.5	< 0.5
NO_3^-	25.66 ± 0.03	3.57 ± 0.002	0.53 ± 0.008
Cl^-	65.91 ± 0.02	10.78 ± 0.008	2.40 ± 0.001
SO_4^{2-}	20.81 ± 0.02	2.68 ± 0.002	6.94 ± 0.002
Conductivity, μS cm^{-1}	147	28.1	84.5
pH	7.4	6.8	5.9

Chemical Surface Characterization

The chemical composition at the surface of the samples was analyzed before corrosion tests by X-ray photoelectron spectroscopy (XPS) using a ThermoFisher Scientific spectrometer, model K-alpha$^+$, operating with a monochromatic Al K-α X-ray source. The spot size was 400 μm and the analysis chamber pressure was 10^{-7} Pa.

Immersion Test

Samples of the 6061 alloy with the two thermomechanical treatments investigated were immersed in the three soil extracts used in this study for 30 days. The exposed area was 1 cm^2 and the test was performed at room temperature (± 22 °C). During the period of immersion, the exposed surfaces were monitored at 5-day intervals. After each period of immersion, the samples were removed from solution and the solution pH was monitored with time of test.

Electrochemical Techniques

The electrochemical tests were carried out using a three-electrode cell configuration. Samples of the 6061 alloy with the two temper conditions were used as working electrodes. The area of the samples exposed to electrolyte (0.05 mol L^{-1} of NaCl) corresponded to 1 cm^2. A platinum wire was used as counter electrode and an Ag/AgCl/KCl(sat) electrode as the reference one. The experiments were performed at room temperature (23 ± 2) °C. Open Circuit Potential (OCP) measurements were obtained during 30 min of immersion in

the different soil extracts. Anodic and cathodic polarization curves were obtained at a scan rate of 0.001 V s^{-1}, respectively, between OCP and 1.0 V, and between OCP and − 1.0 V versus Ag/AgCl,$KCl_{3.5M}$. In order to compare the effect of extract composition on the samples anodic behavior, electrochemical tests were also performed in the various soil extracts of this study.

Results and Discussion

Surface Characterization

Figure 1 shows the surface of the 6061-HCR (Fig. 1a) and 6061-T6 (Fig. 1b) after pickling and neutralization in NaOH and HNO_3 solutions. Surface observation showed the matrix attacked and Si–Fe enriched particles, besides some dissolved particles (yellow arrows). Aluminum is attacked in alkaline solutions, whereas dissolution of Mg enriched particles occurs in both, neutral and acid electrolytes. The grain boundaries of the 6061 alloy in the T6 temper condition were attacked by the pre-treatment solutions. Despite the pickling pre-treatment, EDS analysis showed evenly distributed intermetallic phases in the 6061-T6 alloy. Additionally, the HCR temper condition showed a more homogeneous distribution of intermetallic phases of smaller size compared to the 6061-T6.

The surface chemical composition of the tested samples was characterized by XPS analysis, Fig. 2. The binding energy spectra for the etched surfaces indicated a thicker oxide layer related to the HCR surface than on the T6 one. Higher Cu, Si, Fe, and Mn signals were related to the HCR condition, compared to the T6 one whose surface was enriched in Mg. The Si and Fe signals are mainly related to the intermetallic phases. These results corroborate SEM surface observations. XPS analysis depth is about 8–10 nm. Once Al oxide is naturally air-formed on the Al-alloys, the high Al2*p* signal in the spectra for the HCR condition corresponding to metallic Al peak (71.2 eV) indicates that the thickness of the air-formed oxide on the alloy is very thin [17]. The contribution of oxides and hydroxides in the Al2*p* and O1*s* peaks has been reported [18–22]. A more pronounced signal of Mg was associated with the T6 (1305.38 eV) sample spectrum compared to the HCR

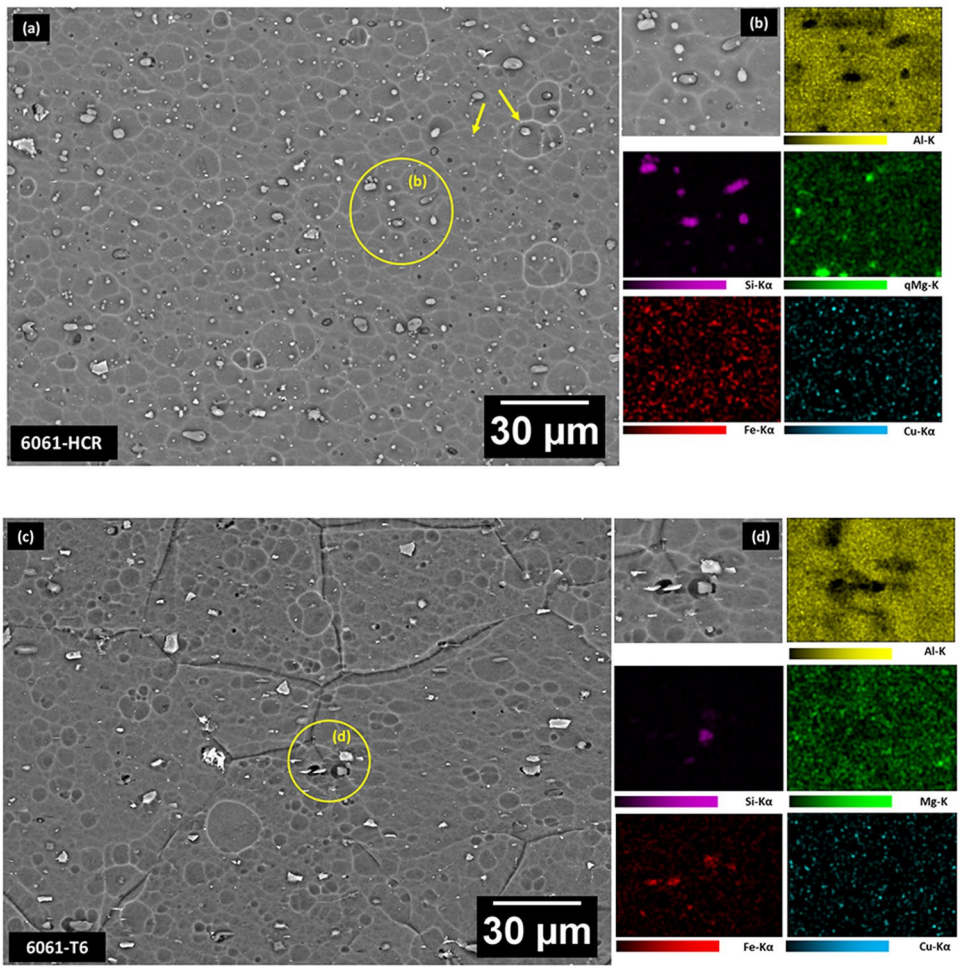

Fig. 1. Surface and EDS image maps of the (**a**, **b**) 6061-HCR and (**c**, **d**) 6061-T6 after pickling and neutralization surface treatments

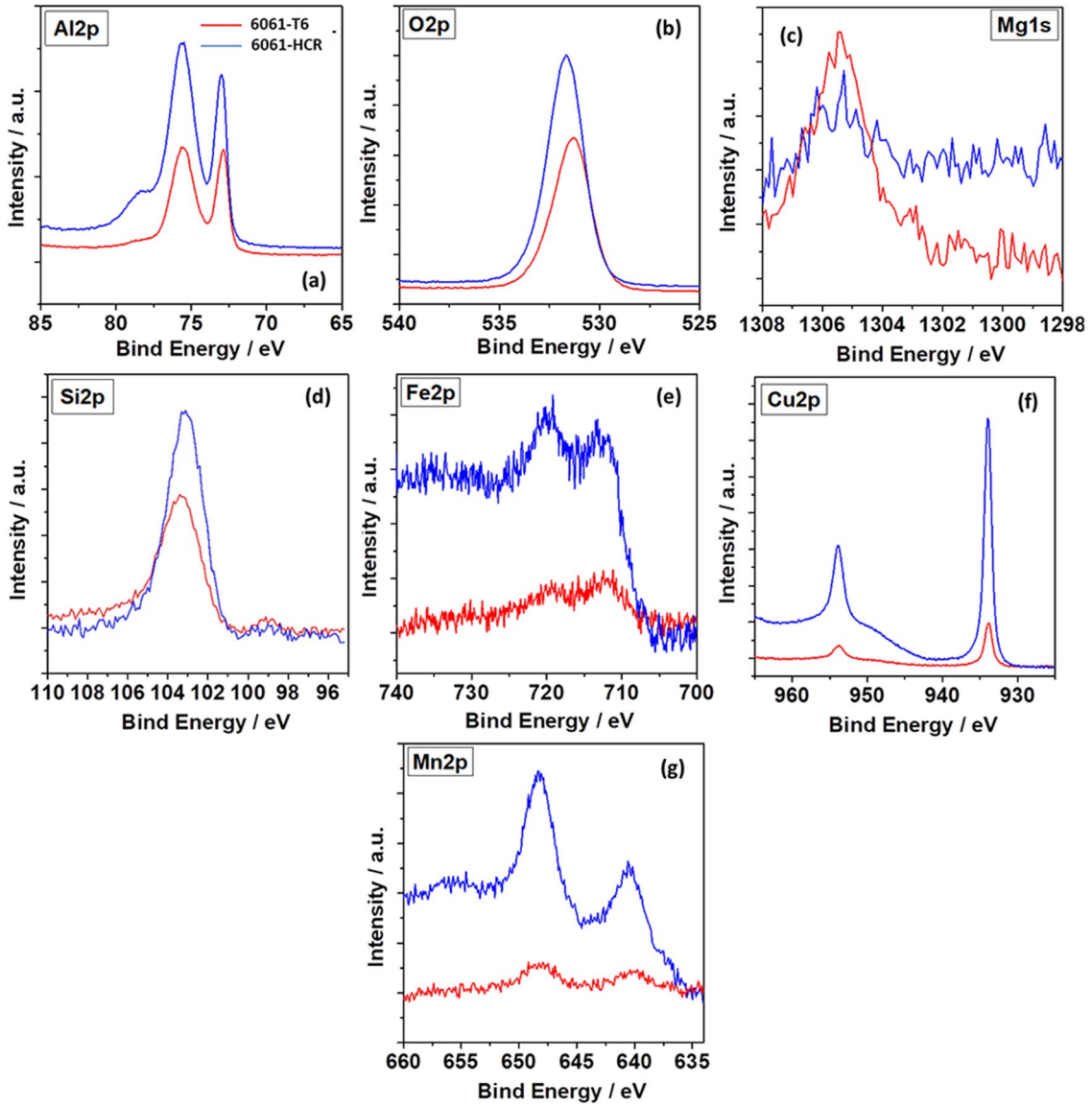

Fig. 2. Surface composition of the 6061-T6 and 6061-HCR alloy after etching obtained by XPS. High-resolution spectra deconvolution was obtained using Al Kα radiation for: (**a**) Al2*p*; (**b**) O2*p*; (**c**) Mg1*s*, (**d**) Si2*p*; (**e**) Fe2*p*; (**f**) Cu2*p*

(1305.28 eV) [23]. The lack of a pronounced Mg peak in the HCR alloy could be related to the better Al oxide film. Since in the T6 temper the density of the Mg enriched second phases is higher than in the HCR condition [9], the more distinct Mg peak for the T6 alloy is observed as these particle acts as defects in the oxide film.

Corrosion Characterization

Figure 3 shows the surface of the 6061-T6 (Fig. 3a) and HCR (Fig. 3b) samples after increasing periods of immersion in the different soil extracts used until a period of 30 days. For both alloys, the oxide growth was suggested from the first days of immersion. Monitoring of the surface with time of test showed that corrosion did not result in significant changes during all period of the test. Despite no significant changes being observed at the surface until 30 days of immersion, there was indication of chemical activity during the whole period of test, as it can be observed by variation in the pH of the solutions, Fig. 4. The highest variations in pH were related to the alloys immersed in the Soil 3 extract. After 30 days of test, the exposed surfaces were observed by scanning electron microscopy (SEM) and analyzed by energy dispersion spectroscopy (EDS), as shown in Figs. 5 and 6. Surrounding the pits, signal of elements such as Fe and SI related to intermetallic phases and oxygen related to

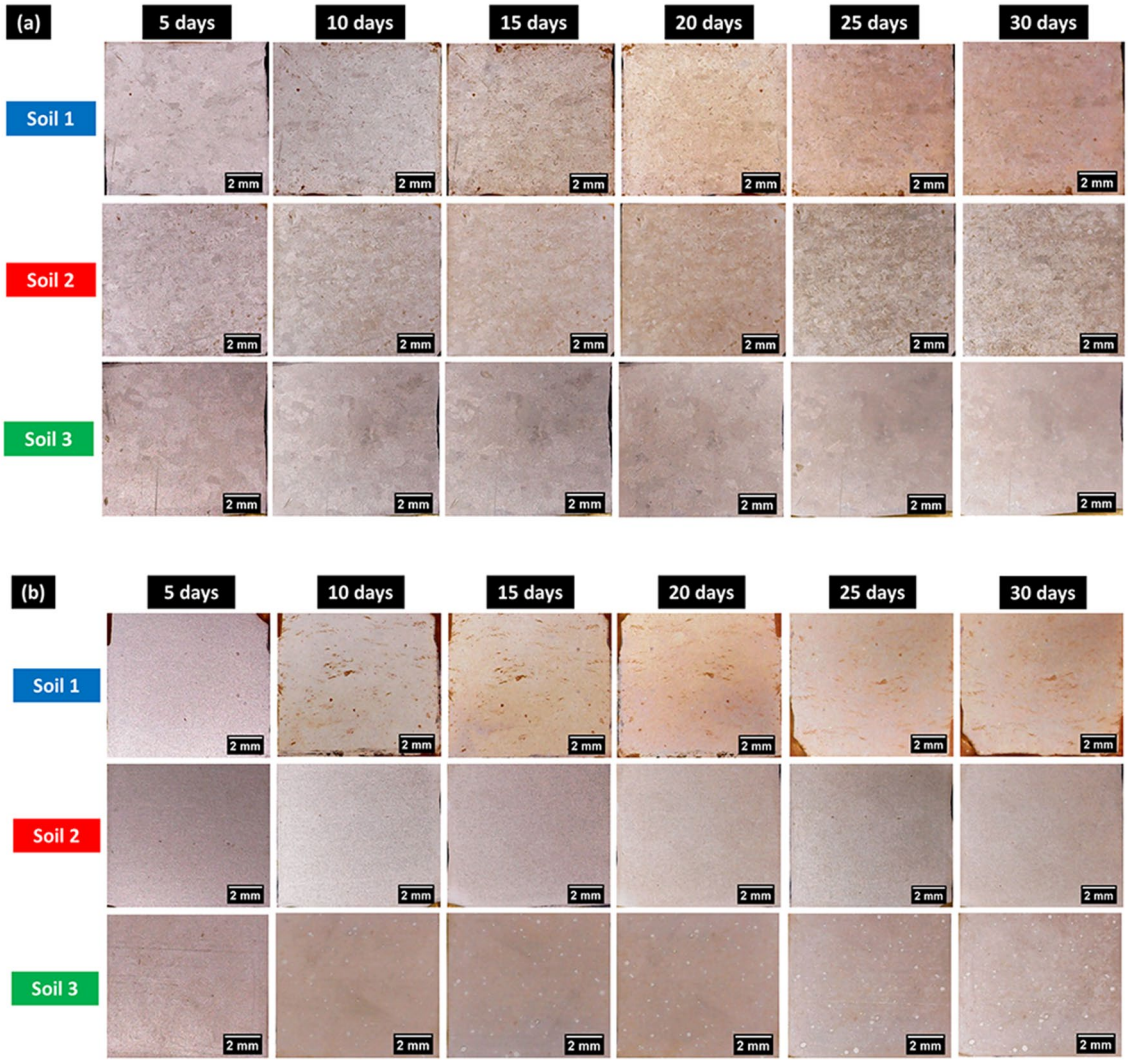

Fig. 3. Surface macrographs of the tested alloys after increasing periods of exposure to the three soil extracts used as corrosion test environment. (**a**) 6061-HCR and (**b**) 6061-T6 alloys

oxides are observed, Fig. 5. The Fe–Si intermetallic phases present in both conditions, T6 and HCR, are cathodic to the matrix and were not attacked during immersion, Fig. 6. However, Mg signals are observed surrounding the pits, Fig. 5, and near the cathodic intermetallic phases, Fig. 6. This behavior was observed for both conditions, T6 and HCR.

In previous works, it was observed that samples of the 6061 alloy with the two tempers, T6 and HCR, are susceptible to corrosion propagation in the 0.05 mol L^{-1} NaCl solution [8]. However, in this work, despite the high concentration of chloride in the soil extracts, no intergranular attack was observed in the 6061-T6 alloy, Fig. 7a. This is due to the etching step that previously attack the grain boundaries, leading to preferential attack inside the grains during the corrosion tests. Surface profile analysis, Fig. 7b, showed that after 30 days of immersion, deep pits were observed in both alloys.

Neutron tomography images (NTI) showed regions of high attenuation coefficients (red regions), Fig. 8. The results corroborate those obtained by 3D profilometry, despite no evidence of corrosion sites by surface observation at low magnification (Fig. 1). Regions with high attenuation coefficients are associated with high hydrogen content. Once Al presents great transparency to neutrons beam, the presence of hydrogen at the corroded regions allows analysis of Al alloys corrosion susceptibility. The arrows, for instance, indicate the highest attenuation values obtained and the thickness of the affected area in each condition. The NTI results support the observations of the effect of soil composition on the corrosion of the 6061 alloy for both tempers, T6 and HCR.

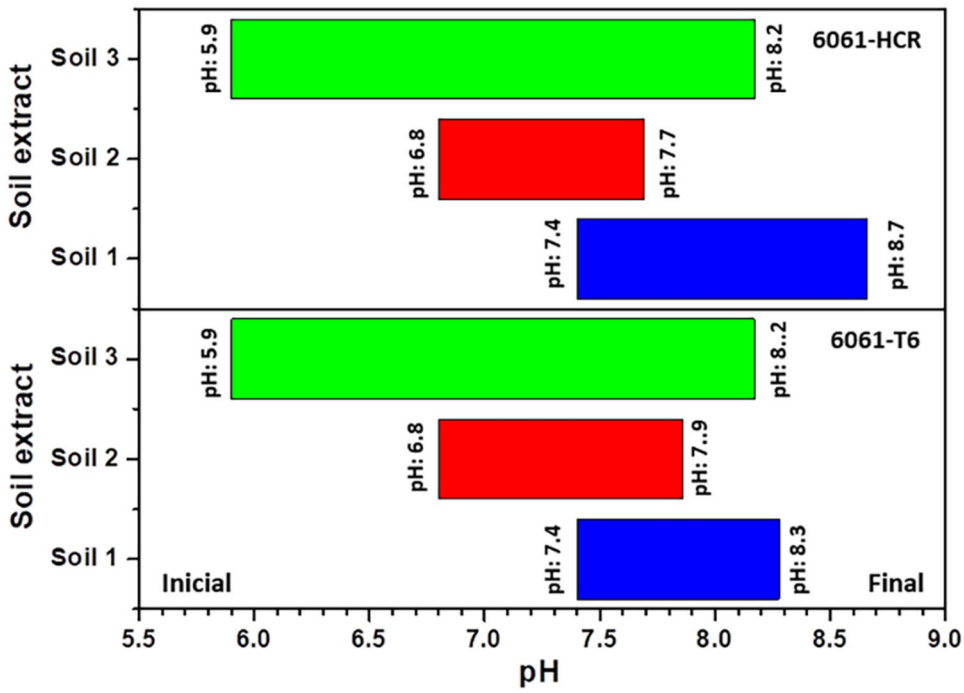

Fig. 4. pH variation of the soil extract exposed to 6061-HCR and 6061-T6 during 30 days of immersion test

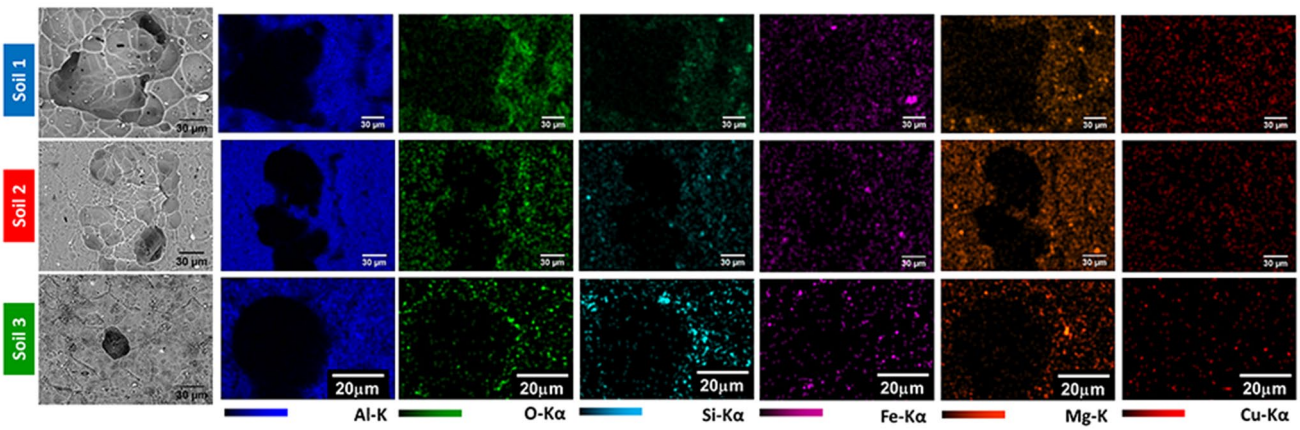

Fig. 5. EDS maps of the 6061-HCR pits after immersion in different soil extracts for 30 days

The kinetics of the corrosion process was evaluated in the various soil extracts by polarization curves, Fig. 9. The results show significant differences in the electrochemical behavior of the 6061 alloy in the two tempers in the three soil extracts. Polarization curves obtained in 0.05 mol L^{-1} NaCl were also obtained and are presented for comparison reasons. The potential for breakdown of the passive film (E_{break}) was dependent on the temper condition for all soil extracts. As shown in Fig. 9a and Table 2, the kinetics of the anodic reactions increase in the following sequence: Soil 1 < Soil 2 < Soil 3. The differences between the OCP and E_{break} values for the HCR and T6 tempers are shown in Fig. 9b. The greater the difference between OCP and E_{break}, the higher the resistance to localized oxide film breakdown. The results indicated lower susceptibility to passive film breakdown related to HCR temper compared to the T6 alloy condition. The polarization curves in 0.05 mol L^{-1} of NaCl solution did not indicate a passive behavior of the 6061 alloy, only a "pseudo passive" behavior in chloride environment showing that the alloy in the two tempers is highly electrochemically active in the presence of chloride but nitrate and sulphate ions act as corrosion inhibitors for this alloy.

Figures 10 and 11 show the alloys surface after anodic polarization test. Pits are observed over all exposed surfaces. Despite the fact that a breakdown potential was not easily

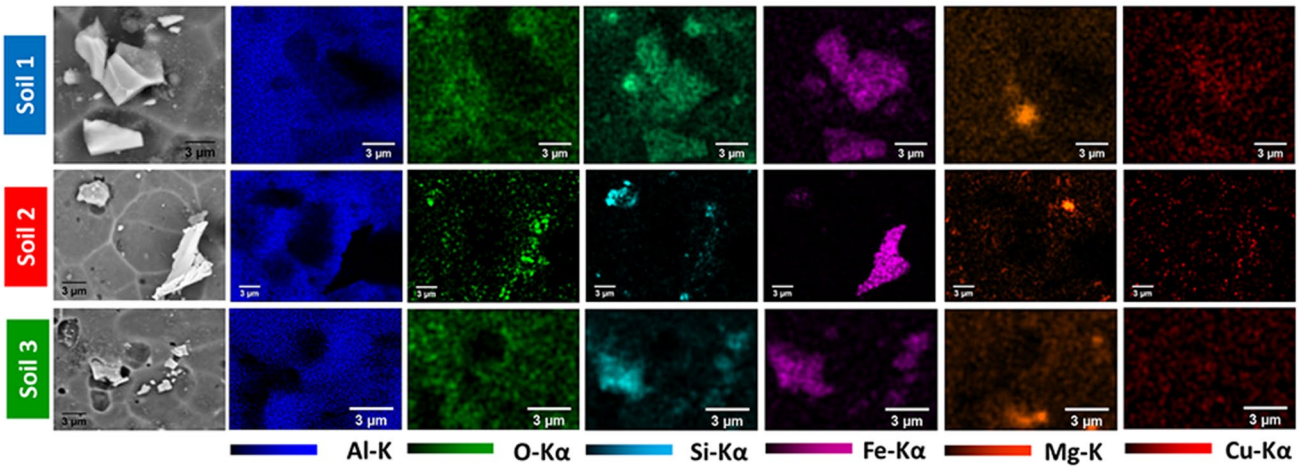

Fig. 6 EDS maps of the 6061-T6 micrometric particles after immersion in different soil extracts for 30 days

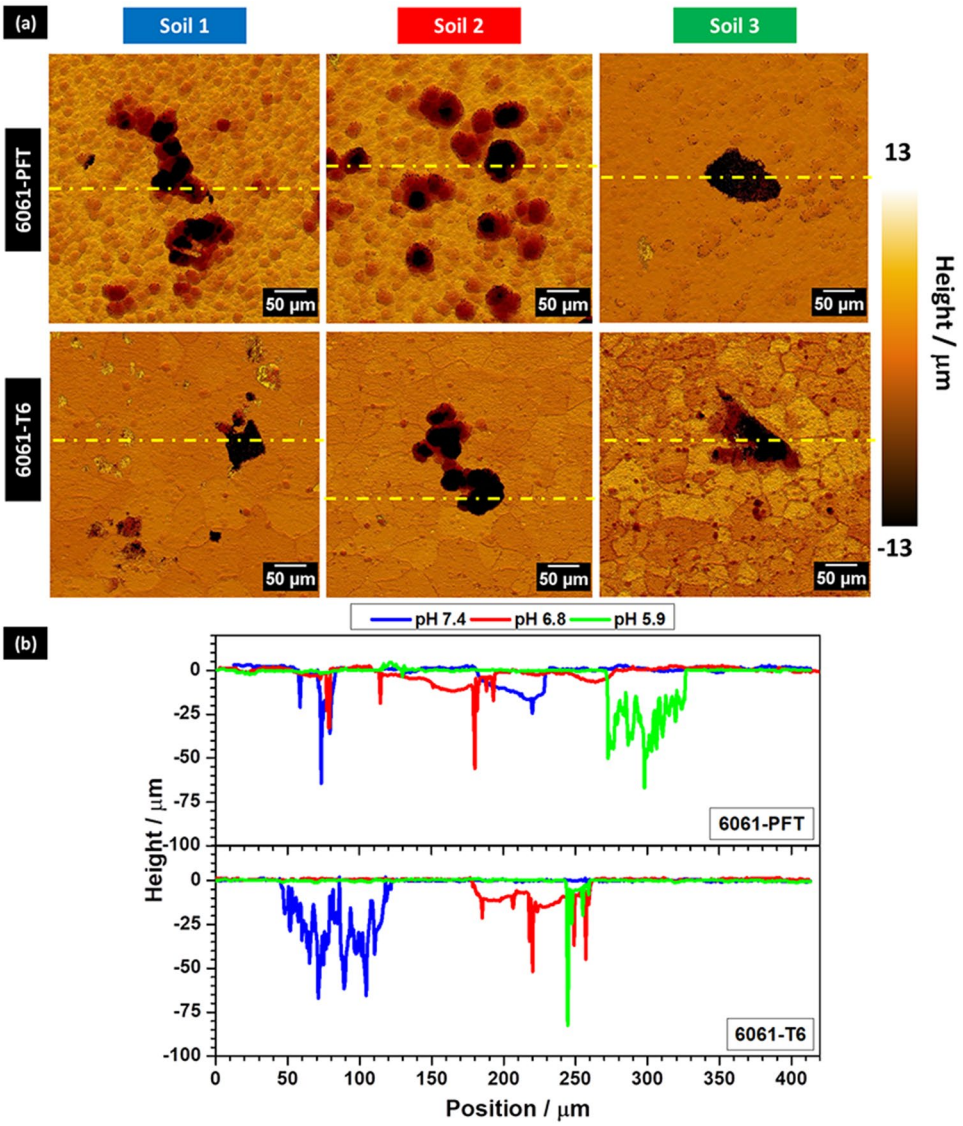

Fig. 7. (**a**) 3D profilometry images of the 6061-HCR and 6061-T6 alloy after 30 days of immersion in the three soil extracts used in this study; (**b**) depth profile at the dashed lines indicated in (**a**) indicating the depth of penetration at the areas of localized attack

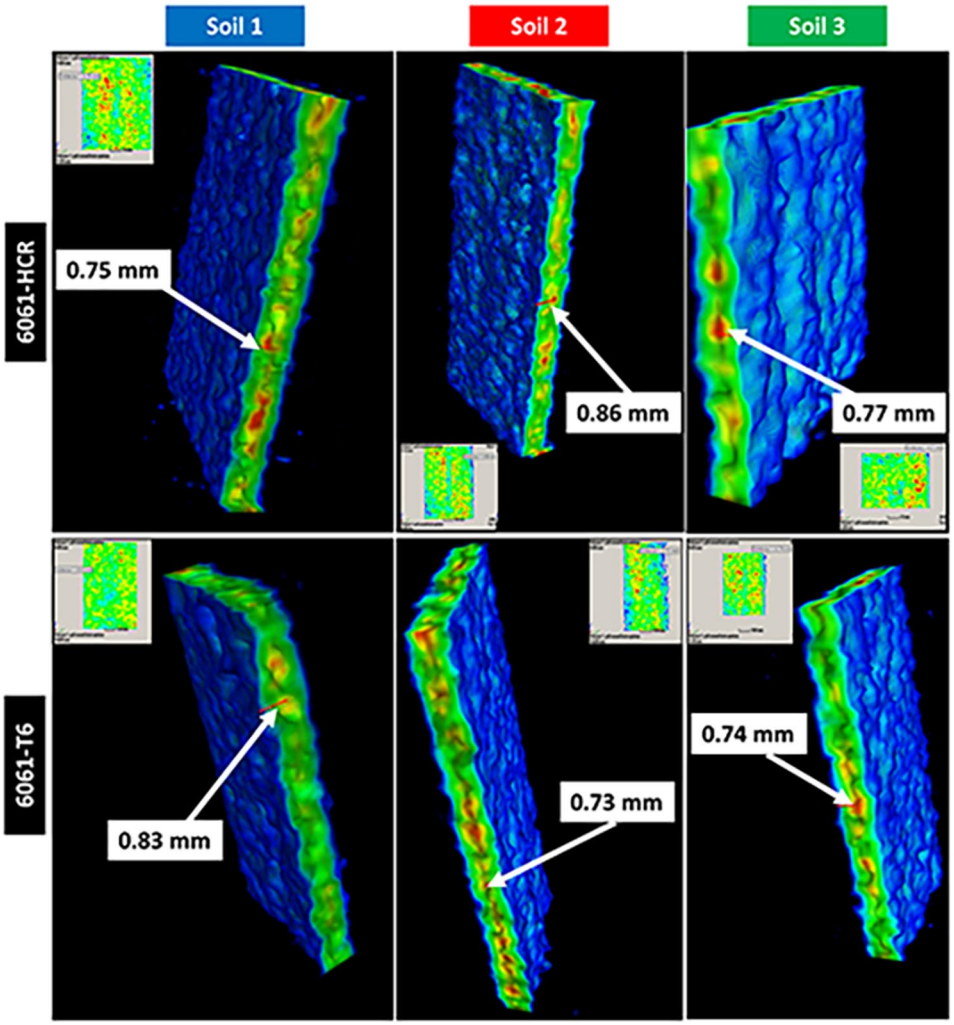

Fig. 8. Neutron 3D tomography images of the 6061-HCR (**a**–**c**) and 6061-T6 (**d**–**f**) after 30 days of immersion in three different soil extracts. The arrows indicate the region with the highest attenuation value and the thickness of the affected area for each condition

identified in the polarization curve corresponding to the T6 condition in Soil 1 extract, Fig. 9, surface observation of the sample after anodic polarization showed pits, Fig. 11a and b. This can be explained by limitation of the polarization technique considering that the current density measured corresponds to a mean of the current produced over the whole exposed surface. Moreover, it was also observed that T6 condition presented susceptibility to intergranular attack when anodically polarized, although this type of attack was not seen in the samples immersed in the soil extracts at the OCP, Fig. 7. The absence of intergranular corrosion in the T6 condition when freely corroding (OCP) is due to the much lower kinetics of corrosion at OCP comparatively to corrosion under anodic polarization. Pickling treatment revealed a preferential attack of the grain boundaries in the T6 alloy showing the susceptibility of the alloy in this condition to intergranular attack.

The cathodic curves were obtained for each alloy in different soil extracts, Fig. 12. According to the results, the kinetics of the cathodic reaction increase as follows Soil 1 < Soil 2 < Soil 3. The highest cathodic currents were related to the T6 condition. Surface observation after cathodic polarization showed precipitation products over the intermetallic phases for both tempers tested, HCR and T6.

Table 1 shows that the soils are mainly composed of chloride, nitrate, and sulfate ions. Chloride ions are highly aggressive to aluminum alloys. Indeed, increase in corrosion rate of the 6061 alloy is related to increments in chloride concentration [25, 26]. Pitting corrosion in chloride environments occurs by adsorption of these ions on the oxide film increasing the susceptibility to passive film breakdown, mainly at defects in the oxide film, and oxygen reduction reaction occurs on the cathodic intermetallic phases until the double layer is charged and the breakdown potential is reached leading to film breakdown [27]. As observed in this study, 3D images profilometry and 3D images tomography showed susceptibility to localized corrosion of the 6061 alloy for the two tempers tested, T6 and HCR. Polarization curves showed significantly lower anodic currents for the 6061 alloy exposed to all soil extracts compared to the

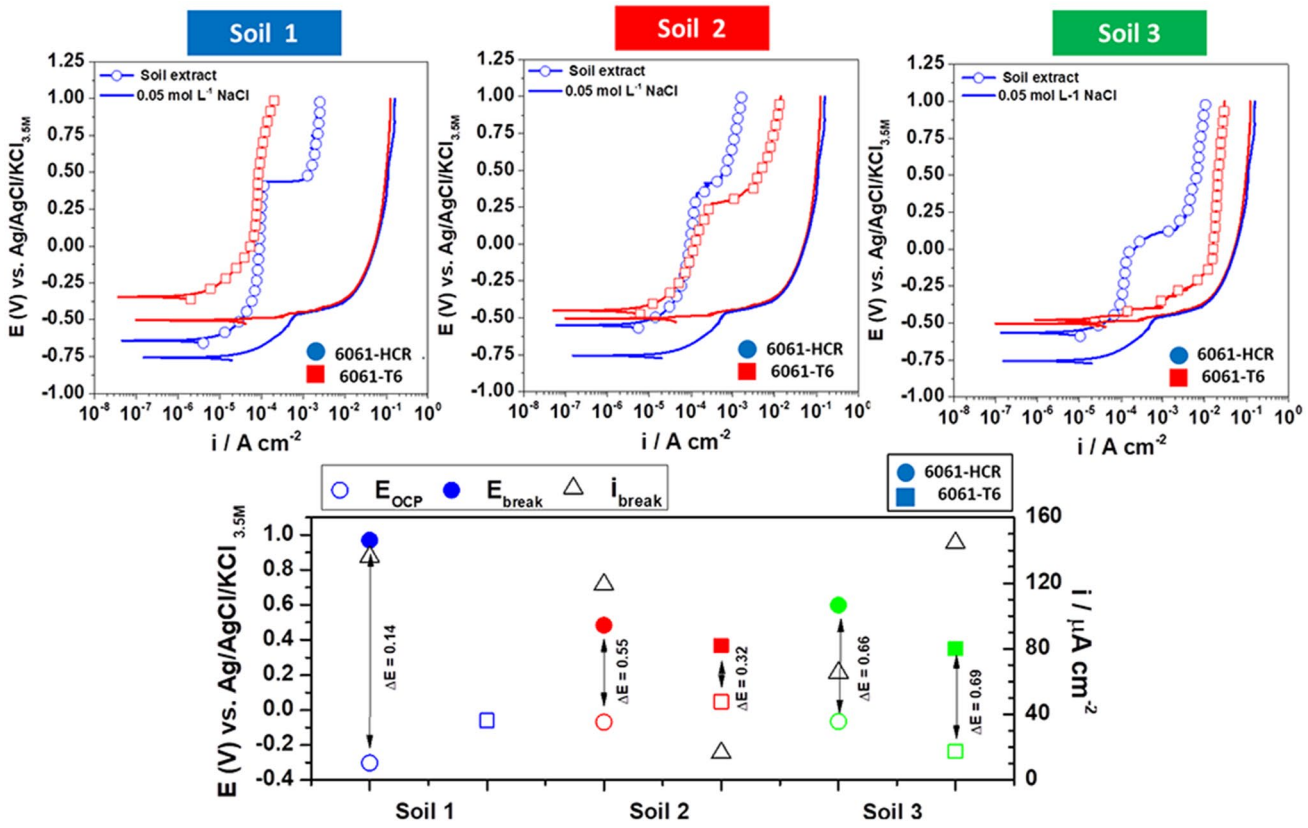

Fig. 9. (**a**) Anodic polarization curves obtained after 30 min of immersion in different soil extracts. Straight lines correspond to anodic curves obtained in 0.05 mol L^{-1} NaCl solution for comparison; (**b**) relation between OCP, breakdown potential (E_{break}), and current density (i_{break}) for the 6061-HCR and 6061-T6 alloys in different soil extracts

Table 2 Corrosion parameters obtained from the anodic polarization test of the 6061-HCR and 6061-T6 immersed in different soil extracts

	E_{OCP}	E_{break}	i_{break}
6061-HRC (Soil 1)	−0.641	0.436	7.50×10^{-4}
6061-T6 (Soil 1)	−0.344	…	…
6061-HRC (Soil 2)	−0.550	0.405	2.22×10^{-4}
6061-T6 (Soil 2)	−0.449	0.278	3.21×10^{-4}
6061-HRC (Soil 3)	−0.565	0.108	7.56×10^{-4}
6061-T6 (Soil 3)	−0.478	−0.420	1.45×10^{-4}

0.05 mol L^{-1} NaCl solution. The literature reported a delay in the uptake of chloride ions in the presence of sulfate ions, leading to reduced corrosion in the sulfate-containing solution [24, 28].

Badawy et al. [24] reported the mechanism of inhibition by sulfate ions due to its absorption on the naturally air-formed oxide film promoting passivation. Foley and Nguyen [29] also related the reduced corrosion rate in solution containing sulfate to the precipitation of Al(OH) SO_4. According to the authors, low free energy was associated with the formation of this compound (Al(OH) SO_4), that acted as a partial barrier reducing the kinetics of the corrosion reactions. Oya et al. [30] reported that the pitting potential became nobler with increase in sulfate ions concentration. Klomjit and Buchheit [31] reported that pitting corrosion of 7075-T6 is suppressed in the presence of sulfate, although the inhibition effect presented a limited range of effectiveness. In general, electrolytes containing sulfate in low concentrations favor pitting, whereas those with high concentrations of sulfate ions, reduce the kinetics of aluminum dissolution. This is due to the low stability of Al^{3+} ion in aqueous solutions resulting in more stable complexes, such as $Al(OH)_4^-$. As the SO_4^{2-} ions concentration increase, other soluble complexes, as $Al(OH)^{2+}$, $Al(OH)_2^{2+}$ and $AlSO_4^+$ are formed and found at the electrolyte/electrode interface. Since the corrosion process is controlled by diffusion, in diluted solutions a great number of water molecules are available to combine with the Al^{3+} transporting this ion to the bulk solution. On the other hand, in highly concentrated solutions, the amount of complex ions at the electrolyte/electrode interface increases and, consequently, the kinetics of corrosion is reduced [32].

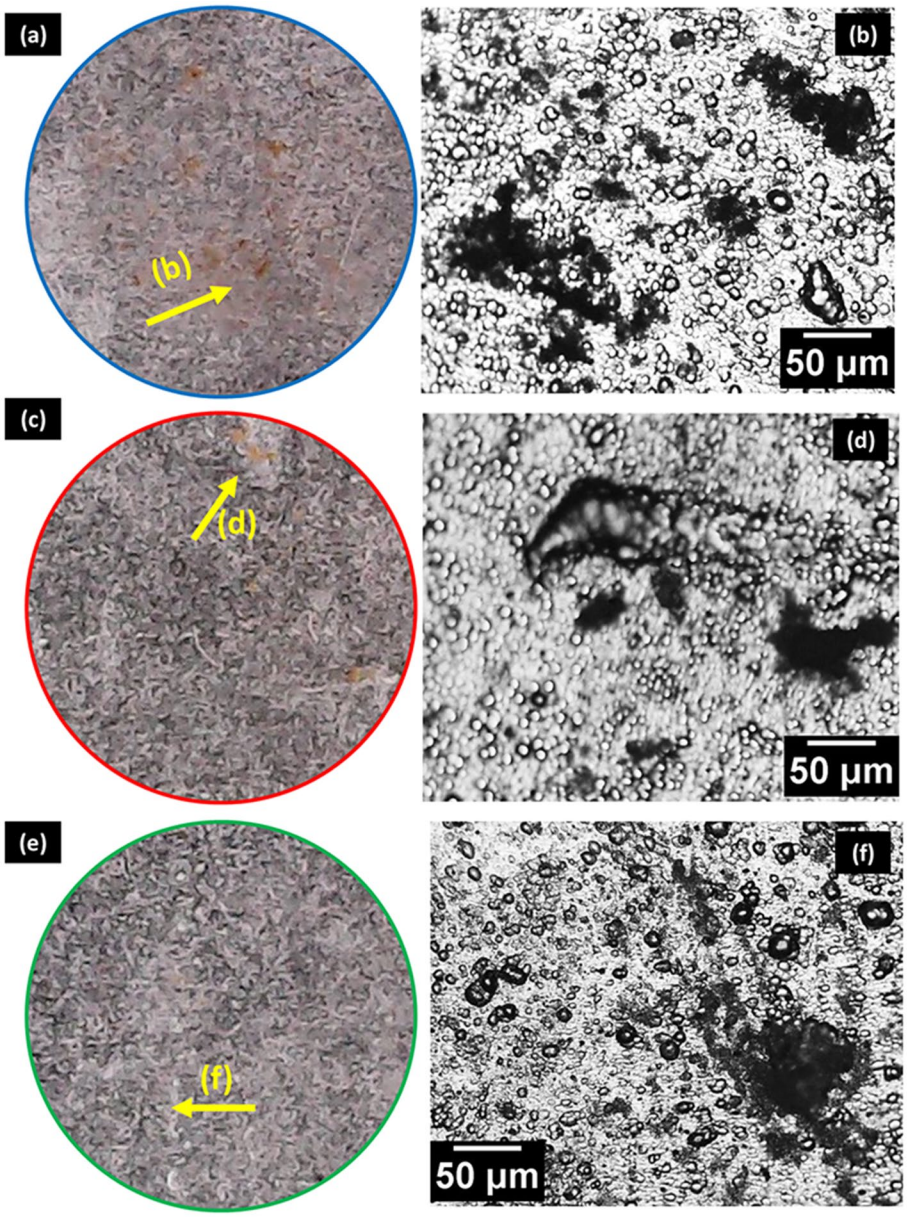

Fig. 10. Surface of the 6061-HCR after anodic polarization in different soil extracts. (**a**, **b**) Soil 1; (**c**, **d**) Soil 2; (**e**, **f**) Soil 3

Ions are reported to play a controversial role in the corrosion of Al alloys [33]. It might improve the performance of passive film reducing the probability of pitting corrosion initiation [32, 34–38], but, might also promote localized corrosion, once stable pits are initiated [33, 39]. According to literature, these ions are not sufficiently aggressive to initiate oxide film breakdown being incorporated into the oxide surface film and increasing the corrosion potential at the surface [40–42]. Samuel et al. [43] reported that certain Cl^-/NO_3^- ratios can accelerate corrosion of Al alloys. At high nitrate concentrations, the reduce corrosion susceptibility reduction has been related to inhibition by their incorporation into the film [41].

The polarization response of the 6061 alloy is strongly influenced by the pH of electrolyte [25, 44]. According to Gupta et al. [44], the anodic reaction kinetics associated with the Mg enriched nano-sized phases is slowed down as the pH increases. For high pH solutions, Mg enriched particles are passive whereas, in neutral/acid environments, the passive behavior is not observed. Similarly, the cathodic reaction kinetics is faster under acidic/neutral conditions. Although the soil extracts used in this work present typically neutral pH, the differences found in corrosion of the tested alloy in the three different soil extracts, are mainly related to the soil extract composition. In this work, a relation was observed between the increase in the SO_4^{2-} to NO_3^- ratio and the decreased susceptibility to

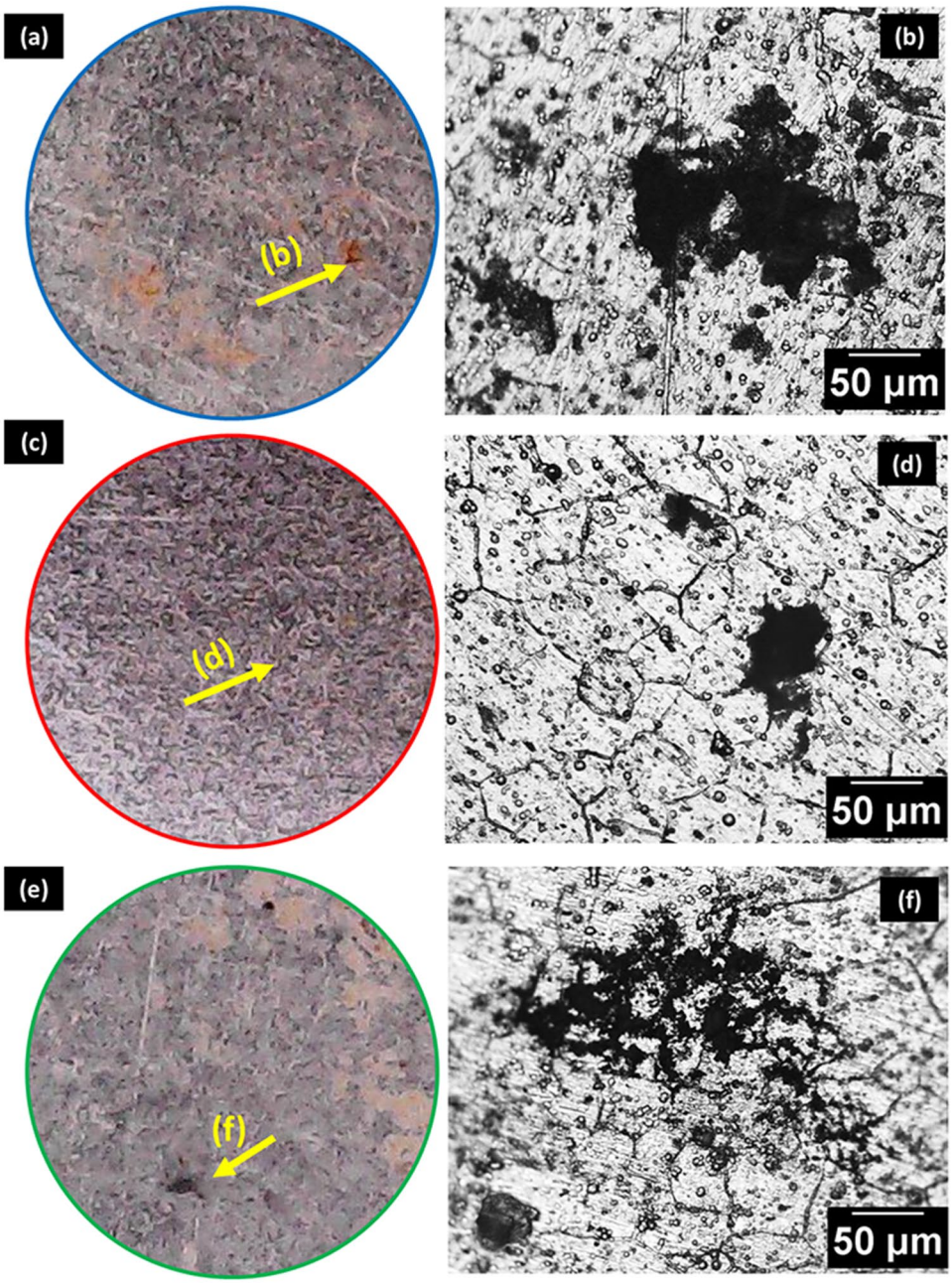

Fig. 11. Surface of the 6061–T6 after anodic polarization in different soil extracts. (**a**, **b**) Soil 1; (**c**, **d**) Soil 2; (**e**, **f**) Soil 3

corrosion. The samples exposed to the soil extract of lowest sulfate and nitrate concentrations, Soil 3, presented the highest susceptibility to corrosion. This is in agreement with the results reported by Samuels et al. [43] showing that higher concentrations of NO_3^- for a same Cl^- concentration, leads to enhanced corrosion resistance. However, the passivating effect of nitrate can lead to increased corrosion attack propagation, once a stable pit is formed. Deep pits were seen in the present study by 3D profilometry. This is explained by the high ratio between the large cathodic areas (passive regions promoted by NO_3^-) and the small anodic sites (pit).

Corrosion susceptibility was dependent on the alloy temper (thermomechanical process). As observed by the XPS results, after pickling treatment the signal corresponding to surface oxide was more intense for the HCR than for the T6. Additionally, the Mg signal was higher for T6 than HCR. A thicker oxide film on the HCR contributes to its higher corrosion resistance compared to the T6. The poor protection of the oxide film in T6 condition formed after pickling contributes to the corrosion process. 3D tomography images showed deeper corrosion penetration for the T6 relatively to HCR one, and this result is supported by previous work [7, 8].

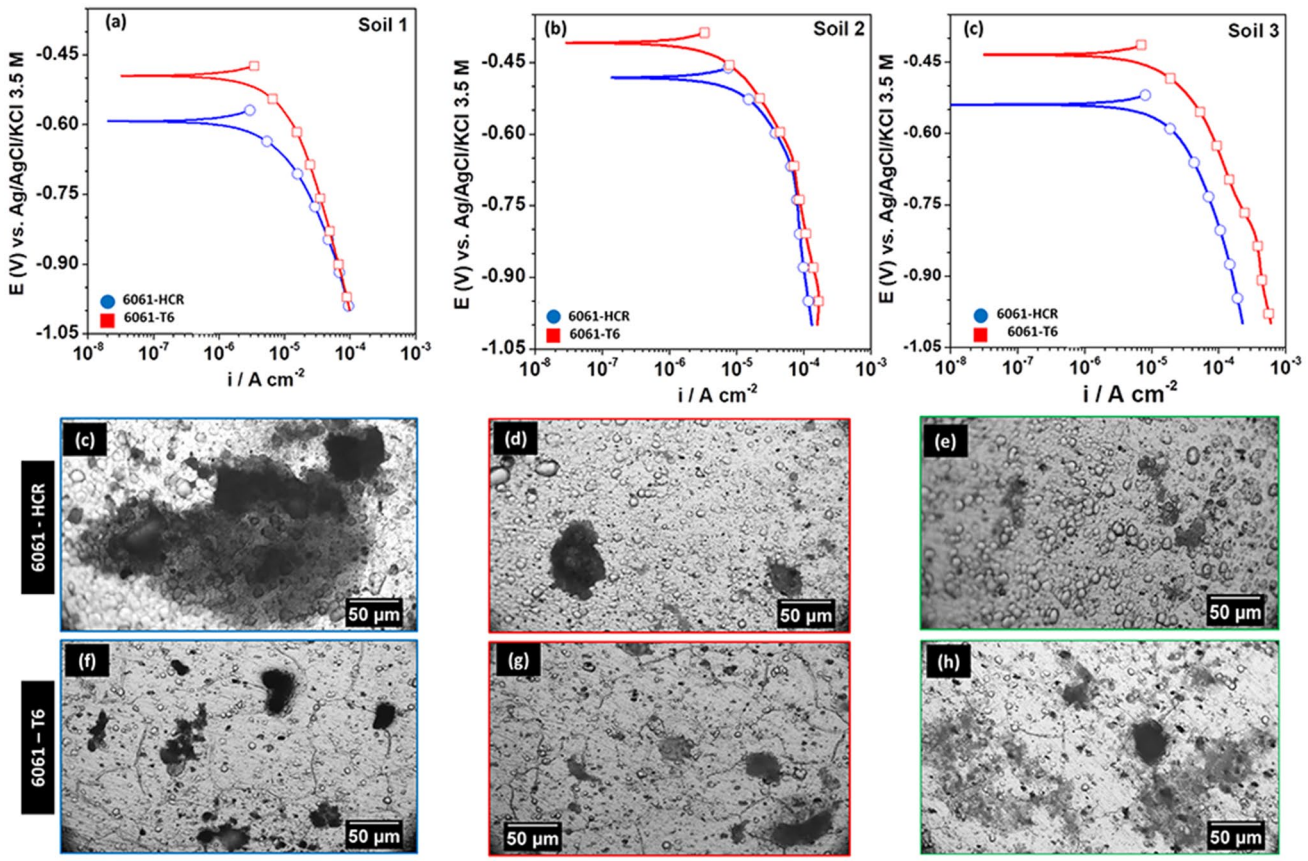

Fig. 12. (**a**) Cathodic polarization curves obtained after 30 min of immersion in different soil extracts and; the exposed surface of the (**b**–**d**) 6061-HCR and (**e**–**g**) 6061-T6 after polarization showing the precipitation products over the particles in each soil extract

It is proposed that the corrosion process of the 6061 alloy is controlled by different processes depending on the thermomechanical treatment. Corrosion in the HCR alloy seems to be controlled by the characteristics of the surface oxide film, as indicated by XPS results. However, for the 6061-T6, its higher amount of Mg-enriched phases is seemingly the main factor controlling the corrosion process. As the pH of the soil extracts was not sufficiently high to maintain the passivity of these phases, preferential dissolution occurs. Although deposition of corrosion products slows down the kinetics of corrosion reaction, inside the pits, the high concentration of chloride and low pH decrease promote pit propagation. For the 6061-HCR alloy, the evenly distributed intermetallic phases favor a more homogenous and thicker oxide film with better corrosion resistance relative to the 6061-T6.

Conclusions

In this work, the corrosion behavior of the 6061 alloy in two different temper conditions, T6 and HCR, was studied in three different soil extracts. The HCR condition presented better corrosion properties compared to the T6. This was due to a thicker and less defective oxide film on the 6061-HCR alloy in relation to the 6061-T6. The higher amount of Mg-enriched particles associated with the T6 condition compared to the HCR resulted in increased corrosion susceptibility for that condition. Increased concentrations of sulfate and nitrate ions in the extract solution resulted in reduced corrosion kinetics of the 6061 alloy in both thermomechanical conditions, T6 or HCR.

Acknowledgements The authors acknowledge the National Commission for Nuclear Energy (CNEN) in Brazil for financial support for this work and for the grant of Mariana X. Milagre (SEI

01342.002357/2019-32). Acknowledgments are also due to Dr. José A. B. de Souza and Dr. Stela M. C. Fernandes of the Instituto de Pesquisas Energéticas e Nucleares (IPEN-CNEN) for providing the material used in this study.

References

1. *ASM Handbook Properties and Selection: Nonferrous Alloys and Special-Purpose Materials* (ASM International, 2001). http://books.google.com.hk/books?id=eC-Zt1J4oCgC
2. J. Buha, R.N. Lumley, A.G. Crosky, K. Hono, Secondary precipitation in an Al–Mg–Si–Cu alloy. Acta Mater. **55**, 3015–3024 (2007). https://doi.org/10.1016/j.actamat.2007.01.006
3. C. Cayron, P.A. Buffat, Transmission electron microscopy study of the β′ phase (Al–Mg–Si alloys) and QC phase (Al–Cu–Mg–Si alloys): ordering mechanism and crystallographic structure. Acta Mater. **48**, 2639–2653 (2000). https://doi.org/10.1016/S1359-6454(00)00057-4
4. V. Massardier, T. Epicier, Study of influence of low copper addition and of an excess of silicon on the precipitation kinetics and on the precipitation sequence of Al–Mg_2Si alloys. Mater. Sci. Forum. **396–402**, 851–856 (2002). https://doi.org/10.1007/978-1-4614-7990-1
5. M. Durazzo, P.E. Umbehaun, W.M. Torres, J.A.B. Souza, D.G. Silva, D.A. Andrade, Procedures for manufacturing an instrumented nuclear fuel element. Prog. Nucl. Energy. **113**, 166–174 (2019). https://doi.org/10.1016/j.pnucene.2019.01.021
6. M. Durazzo, J.A.B. Souza, E.F.U. de Carvalho, H.G. Riella, Effect of porosity on the manufacturing of U_3O_8-Al dispersion fuel plates. Prog. Nucl. Energy. **99**, 49–58 (2017). https://doi.org/10.1016/j.pnucene.2017.05.001
7. M.X. Milagre, U. Donatus, R. Maria, P. Silva, J. Victor, S. Araujo, R.M. Souto, I. Costa, Galvanic coupling effects on the corrosion behavior of the 6061 aluminum alloy used in research nuclear reactors. J. Nucl. Mater. **541**, 152440 (2020). https://doi.org/10.1016/j.jnucmat.2020.152440
8. M.X. Milagre, U. Donatus, N.V. Mogili, C.S.C. Machado, J.V.S. Araujo, R.E. Klumpp, S.M.C. Fernandes, J.A.B. de Souza, I. Costa, Effects of picture frame technique (PFT) on the corrosion behavior of 6061 aluminum alloy. J. Nucl. Mater. **539**, 152320 (2020)
9. W.J. Schwerdtfeger, Effects of cathodic currents on the corrosion of an aluminum alloy. J. Res. Natl. Bur. Stand. Eng. Instrum. **68C**, 283–296 (1964)
10. T.A. Lowe, A.H. Koepf, Corrosion performance of aluminum culvert. Highw. Res. Rec. **56**, 98–115 (1964)
11. S. Cheng, L. Hongxi, G. Liqun, Z. Shuquan, Corrosion behavior of LY11 aluminum alloy in soil. Trans. Nonferrous Met. Soc. China. **9**, 796–798 (1999)
12. F. Yan, X. Wang, X. Li, C. Wang, B. Jiang, Corrosion behavior of Al-Cu-RE (Re = La, Ce) alloy joints in alkaline soil extract. Int. J. Electrochem. Sci. **15**, 8012–8025 (2020). https://doi.org/10.20964/2020.08.07
13. F. Yan, X. Wang, X. Wang, X. Li, C. Wang, Effect of shot peening and pre-oxidation duplex treatment on electrochemical corrosion behavior of Al alloy in alkaline soil. Int. J. Electrochem. Sci. **12**, 11212–11223 (2017). https://doi.org/10.20964/2017.12.60
14 R.M. Schoueri, C. Domienikan, F. de Toledo, M.L.G. Andrade, M.A. Stanojev Pereira, R. Pugliesi, The new facility for neutron tomography of IPEN-CNEN/SP and its potential to investigate hydrogenous substances. Appl. Radiat. Isot. **84**, 22–26 (2014). https://doi.org/10.1016/j.apradiso.2013.10.019
15 R. Pugliesi, M.A.S. Pereira, M.L.G. Andrade, J.M.L. Basso, C.G. Voltani, I.C. Gonzales, Study of the fish fossil Notelops brama from Araripe-Basin Brazil by neutron tomography. Nucl. Instrum. Methods Phys. Res. Sect. A Accel. Spectrom. Detect. Assoc. Equip. **919**, 68–72 (2019). https://doi.org/10.1016/j.nima.2018.12.001
16. R.P. Ugliesi, M.L.G.A. Ndrade, M.A.S.P. Ereira, R.M.S. Choueri, M.S.D. Ias, Scientific reviews neutron imaging at the IPEN-CNEN/SP and its use in technology. Neutron News. **25**, 40–44 (2014)
17. R. Ngongang, E. Marceau, X. Carrier, C.M. Pradier, C. Methivier, J.L. Blanc, M. Carre, Surface passivation of aluminum alloy 6061 with gaseous trichlorosilane: a surface investigation. Appl. Surf. Sci. **292**, 165–173 (2014). https://doi.org/10.1016/j.apsusc.2013.11.107
18. P. Traverso, A.M. Beccaria, Effect of magnesium ions on the protective power of corrosion products formed on the surface of Al 6061 T6 alloy–10% Al_2O_3 (v/v) composite in solutions containing chlorides. Surf. Interface Anal. **26**, 524–530 (1998). https://doi.org/10.1002/(sici)1096-9918(199806)26:7%3c524::aid-sia401%3e3.3.co;2-m
19. N.J. Havercroft, P.M.A. Sherwood, Use of differential surface charging to separate chemical differences in x-ray photoelectron spectroscopy. Surf. Interface Anal. **29**, 232–240 (2000). https://doi.org/10.1002/(SICI)1096-9918(200003)29:3%3c232::AID-SIA731%3e3.0.CO;2-6
20. N. Saleema, D.K. Sarkar, R.W. Paynter, D. Gallant, M. Eskandarian, A simple surface treatment and characterization of AA 6061 aluminum alloy surface for adhesive bonding applications. Appl. Surf. Sci. **261**, 742–748 (2012). https://doi.org/10.1016/j.apsusc.2012.08.091
21. S.-S. Wang, F. Yang, G.S. Frankel, Effect of altered surface layer on localized corrosion of aluminum alloy 2024. J. Electrochem. Soc. **164**, C317–C323 (2017). https://doi.org/10.1149/2.1541706jes
22. P. Du, J. Li, Y. Zhao, Y. Dai, Z. Yang, Y. Tian, Corrosion characteristics of Al alloy/galvanized-steel couple in NaCl solution. Int. J. Electrochem. Sci. **13**, 11164–11179 (2018). https://doi.org/10.20964/2018.11.99
23. B. Zaid, N. Maddache, D. Saidi, N. Souami, N. Bacha, A. Si Ahmed, Electrochemical evaluation of sodium metabisulfite as environmentally friendly inhibitor for corrosion of aluminum alloy 6061 in a chloride solution. J. Alloys Compd. **629**, 188–196 (2015). https://doi.org/10.1016/j.jallcom.2015.01.003
24. W.A. Badawy, F.M. Al-Kharafi, A.S. El-Azab, Electrochemical behaviour and corrosion inhibition of Al, Al-6061 and Al–Cu in neutral aqueous solutions. Corros. Sci. **41**, 709–727 (1999). https://doi.org/10.1016/S0010-938X(98)00145-0
25. I.W. Huang, B.L. Hurley, F. Yang, R.G. Buchheit, Dependence on temperature, pH, and Cl^- in the uniform corrosion of aluminum alloys 2024–T3, 6061–T6, and 7075–T6. Electrochim. Acta. **199**, 242–253 (2016). https://doi.org/10.1016/j.electacta.2016.03.125
26. Z. Zhang, Z. Xu, J. Sun, M. Zhu, Q. Yao, D. Zhang, B. Zhang, K. Xiao, J. Wu, Corrosion behaviors of AA5083 and AA6061 in artificial seawater: effects of Cl^-, HSO_3^- and temperature. Int. J. Electrochem. Sci. **15**, 1218–1229 (2020). https://doi.org/10.20964/2020.02.01
27. M.C. Reboul, B. Baroux, Metallurgical aspects of corrosion resistance of aluminium alloys. Mater. Corros. **62**, 215–233 (2011). https://doi.org/10.1002/maco.201005650
28 A. Berzins, R.T. Lowson, K.J. Mirams, Aluminium corrosion studies. III* Chloride adsorption isotherms on corroding aluminium. Aust. J. Chem. **30**, 1891–1903 (1977). https://doi.org/10.1071/CH9771891
29 R.T. Foley, T.H. Nguyen, Chemical nature of aluminum corrosion—5. Energy transfer in aluminum dissolution. Proc. Electrochem. Soc. **81–8**, 27–36 (1982). https://doi.org/10.1149/1.2123881

30 Y. Oya, Y. Honkawa, Y. Kojima, Pitting corrosion of aluminum alloy in chloride solution cantaining sulfate and sulfite ion. Zair Kankyo Corros. Eng. **63**, 394–400 (2014)
31. P. Klomjit, R.G. Buchheit, Localized corrosion inhibition of AA7075-T6 by calcium sulfate. Corrosion. **72**, 486–499 (2016). https://doi.org/10.5006/1892
32. S. Li, B.C. Church, Effects of sulfate and nitrate anions on aluminum corrosion in slightly alkaline solution. Appl. Surf. Sci. **440**, 861–872 (2018). https://doi.org/10.1016/j.apsusc.2018.01.108
33. X. Liu, Y. Li, L. Lei, X. Wang, The effect of nitrate on the corrosion behavior of 7075–T651 aluminum alloy in the acidic NaCl solution. Mater. Corros. **72**, 1478–1487 (2021). https://doi.org/10.1002/maco.202112280
34. E. Samiento-Bustos, J.G.G. Rodriguez, J. Uruchurtu, G. Dominguez-Patiño, V.M. Salinas-Bravo, Effect of inorganic inhibitors on the corrosion behavior of 1018 carbon steel in the LiBr + ethylene glycol + H_2O mixture. Corros. Sci. **50**, 2296–2303 (2008). https://doi.org/10.1016/j.corsci.2008.05.014
35. I.L. Lehr, S.B. Saidman, Characterisation and corrosion protection properties of polypyrrole electropolymerised onto aluminium in the presence of molybdate and nitrate. Electrochim. Acta. **51**, 3249–3255 (2006). https://doi.org/10.1016/j.electacta.2005.09.017
36. M.H. Gao, S.D. Zhang, B.J. Yang, S. Qiu, H.W. Wang, J.Q. Wang, Prominent inhibition efficiency of sodium nitrate to corrosion of Al-based amorphous alloy. Appl. Surf. Sci. **530**, 147211 (2020). https://doi.org/10.1016/j.apsusc.2020.147211
37. J. Datta, B. Samanta, A. Jana, S. Sinha, C. Bhattacharya, S. Bandyopadhyay, Role of Cl^- and NO_3^- ions on the corrosion behavior of 20% SiCp reinforced 6061-Al metal matrix composite: a correlation between electrochemical studies and atomic force microscopy. Corros. Sci. **50**, 2658–2668 (2008). https://doi.org/10.1016/j.corsci.2008.06.027
38. S.N. Afzal, M.A.A. Shaikh, C.M. Mustafa, M. Nabi, M.Q. Ehsan, A.H. Khan, Study of aluminum corrosion in chloride and nitrate media and its inhibition by nitrite. J. Nepal Chem. Soc. **22**, 26–33 (2007)
39. C. Blanc, S. Gastaud, G. Mankowski, Mechanistic studies of the corrosion of 2024 aluminum alloy in nitrate solutions. J. Electrochem. Soc. **150**, B396 (2003). https://doi.org/10.1149/1.1590327
40. I. Milošev, B. Volarič, Conversion coatings based on rare earth nitrates and chlorides for corrosion protection of aluminum alloy 7075–T6. Corrosion. **73**, 822–843 (2017). https://doi.org/10.5006/2353
41 S. Il Pyun, S.M. Moon, The inhibition mechanism of pitting corrosion of pure aluminum by nitrate and sulfate ions in neutral chloride solution. J. Solid State Electrochem. **3**, 331–336 (1999). https://doi.org/10.1007/s100080050163
42. B.L. Treu, S. Joshi, W.R. Pinc, M.J. O'Keefe, W.G. Fahrenholtz, Characterization of localized surface states of Al 7075–T6 during deposition of cerium-based conversion coatings. J. Electrochem. Soc. **157**, C282 (2010). https://doi.org/10.1149/1.3454236
43. B.W. Samuels, K. Sotoudeh, R.T. Foley, Inhibition and acceleration of aluminum corrosion. Corrosion. **37**, 92–97 (1981). https://doi.org/10.5006/1.3593852
44. R.K. Gupta, N.L. Sukiman, K.M. Fleming, M.A. Gibson, N. Birbilis, Electrochemical behavior and localized corrosion associated with Mg_2Si particles in Al and Mg alloys. ECS Electrochem. Lett. **1**, 2–4 (2012). https://doi.org/10.1149/2.002201eel